

# Electronic and Structural Evolution of Monoiron Sulfur Clusters, $\text{FeS}_n^-$ and $\text{FeS}_n$ ( $n = 1-6$ ), from Anion Photoelectron Spectroscopy

Hua-Jin Zhai, Boggavarapu Kiran, and Lai-Sheng Wang\*

Department of Physics, Washington State University, 2710 University Drive, Richland, Washington 99352, and W. R. Wiley Environmental Molecular Sciences Laboratory, Pacific Northwest National Laboratory, MS K8-88, P.O. Box 999, Richland, Washington 99352

Received: December 31, 2002; In Final Form: February 19, 2003

We report a photoelectron spectroscopic investigation of a series of monoiron–sulfur clusters  $\text{FeS}_n^-$  ( $n = 1-6$ ) at various photon energies. Vibrationally resolved spectra were measured for  $\text{FeS}^-$  and  $\text{FeS}_3^-$ . A wealth of electronic structure information was obtained for  $\text{FeS}$  and were tentatively assigned, yielding a  $^5\Delta$  ground state for  $\text{FeS}$  and a  $^7\Sigma^+$  and a  $^5\Delta$  excited state at 0.675 and 1.106 eV above the ground state, respectively. Franck–Condon factor simulations were performed for the vibrationally resolved  $^5\Delta$  ground state and the  $^5\Delta$  excited state, yielding an Fe–S bond length of 2.18 and 2.29 Å for the anion ground state and the  $^5\Delta$  excited state, respectively, as well as a vibrational temperature of 180 K for the anion. The electron affinities (EA's) of  $\text{FeS}_n$  were measured to be  $1.725 \pm 0.10$ ,  $3.222 \pm 0.009$ ,  $2.898 \pm 0.008$ ,  $3.129 \pm 0.008$ ,  $3.262 \pm 0.010$ , and  $3.52 \pm 0.02$  eV for  $n = 1-6$ , respectively. A significant EA increase was only observed from  $\text{FeS}$  to  $\text{FeS}_2$ , whereas all larger species  $\text{FeS}_n$  ( $n = 3-6$ ) possess EA's similar to that of  $\text{FeS}_2$  within  $\pm 0.3$  eV. By comparing the trend of EA in  $\text{FeS}_n$  to that of  $\text{FeO}_n$ , we proposed that all the  $\text{FeS}_n^-$  ( $n > 1$ ) species take  $(\text{S}_m^{2-})\text{Fe}^{3+}(\text{S}_{n-m}^{2-})$  type structures, in which Fe assumes its favorite +3 formal oxidation state. Preliminary density functional calculations were carried out and the obtained structures support the proposed structural evolution of the  $\text{FeS}_n^-$  clusters.

## 1. Introduction

Iron–sulfur clusters are prevalent throughout bioinorganic chemistry.<sup>1</sup> Abiological investigations of iron–sulfur clusters and complexes<sup>2–5</sup> provide fundamental information about the structural, electronic, and magnetic properties, and chemical bonding of the Fe–S systems. A large number of iron–sulfur clusters and complexes have been synthesized and characterized, forming a large class of organometallic chemistry.<sup>2</sup> There have also been extensive theoretical efforts devoted to iron–sulfur complexes.<sup>3–5</sup> However, there have been relatively few studies on the bare Fe–S clusters; even the electronic structure of the simplest  $\text{FeS}$  diatomic molecule is still not well understood. We are interested in probing the electronic structure and chemical bonding of a broad range of iron–sulfur systems in the gas phase using photoelectron spectroscopy (PES), ranging from bare Fe–S clusters produced using a laser vaporization source<sup>6</sup> to analogue complexes and proteins using an electrospray ionization source.<sup>7</sup> In the current paper, we focus on a series of relatively simple bare iron–sulfur clusters, the monoiron sulfur clusters  $\text{FeS}_n^-$  ( $n = 1-6$ ).

There have been numerous experimental and theoretical reports on the monoiron–sulfur clusters in the literature. DeVore et al. reported a vibrational frequency of  $540 \text{ cm}^{-1}$  for neutral diatomic  $\text{FeS}$  using matrix infrared spectroscopy.<sup>8</sup> The reactions of  $\text{FeS}^+$  with  $\text{D}_2$  and methane were examined by Barsch et al. using guided-ion beam mass spectrometry.<sup>9,10</sup> Photodissociation spectra of  $\text{FeS}^+$  were measured by Hettich et al.<sup>11</sup> and Husband et al.<sup>12</sup> Schröder et al. have reported a detailed study on the structures of cationic, anionic, and neutral  $\text{FeS}_2$  using both mass spectrometric methods and density functional theory (DFT)

calculations.<sup>13</sup> Sequential reactions of  $\text{Fe}^+$  with ethylene sulfide were conducted to generate  $\text{FeS}_n^+$  species, and at least six sulfur attachments were observed.<sup>14</sup> Bare  $\text{Fe}^+$  ions were also allowed to react with  $\text{S}_8$  in the gas phase using a Fourier transform ion cyclotron resonance mass spectrometer to produce  $\text{FeS}_n^+$  clusters,<sup>15,16</sup> and species with  $n$  up to 10 were observed. Photodissociation and collision-induced dissociation (CID) experiments were carried out on  $\text{FeS}_n^+$  ( $n = 1-6$ ) by MacMahon et al.,<sup>17</sup> and on  $\text{FeS}_n^+$  ( $n = 2-8$ ) by Yu et al.<sup>18</sup> Anionic  $\text{FeS}_6^-$  and  $\text{FeS}_7^-$  were also investigated by CID, and loss of neutral  $\text{S}_2$  fragments were observed as a major dissociation channel.<sup>19</sup> Low resolution photoelectron spectra of  $\text{FeS}_n^-$  ( $n = 1-6$ ) at 266 nm were reported by Kaya and co-workers.<sup>20</sup> Theoretical treatment of iron–sulfur clusters has been challenging.<sup>3–5,21–26</sup> Even the electronic structure and chemical bonding in the diatomic  $\text{FeS}$  were not well understood at present despite much effort in the past decade.<sup>21–25</sup> Except for the DFT calculations of  $\text{FeS}_2$  by Schröder et al.,<sup>13</sup> there is no other theoretical studies on any other larger  $\text{FeS}_n$  clusters.

In this paper, we report a detailed photoelectron spectroscopic study of a series of monoiron–sulfur clusters:  $\text{FeS}_n^-$  ( $n = 1-6$ ). Vibrationally resolved PES spectra and studies at various photon energies allow a wealth of information on the structural and electronic evolution and chemical bonding in the monoiron–sulfur clusters to be obtained. The  $\text{FeS}_n^-$  clusters were compared with the  $\text{FeO}_n^-$  species and they were proposed to have  $(\text{S}_m^{2-})\text{Fe}^{3+}(\text{S}_{n-m}^{2-})$  types of structures, in which the Fe atom assumes its favorite formal oxidation state of +3. A preliminary DFT study was carried out on the structures of  $\text{FeS}_n^-$  and the DFT results are consistent with the proposed structural evolution for the monoiron–sulfur clusters.

\* Corresponding author. E-mail: ls.wang@pnl.gov.

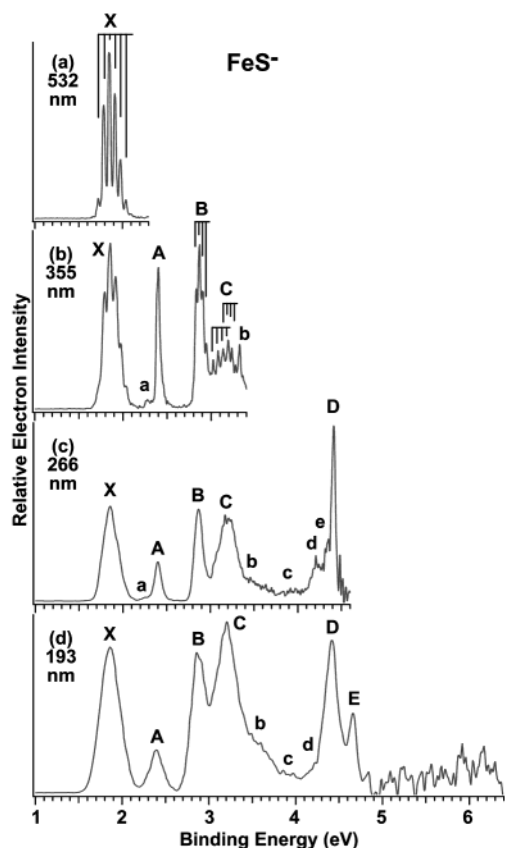


**Figure 1.** Photoelectron spectra of  $\text{FeS}^-$  at (a) 532 nm (2.331 eV), (b) 355 nm (3.496 eV), (c) 266 nm (4.661 eV), and (d) 193 nm (6.424 eV). The vertical lines represent vibrational structures.

## 2. Experimental Method

The experiment was carried out using a magnetic-bottle time-of-flight PES apparatus equipped with a laser vaporization supersonic cluster source.<sup>6</sup> Briefly, a mixed Fe/S target (10/1 molar ratio) was laser-vaporized in the presence of a helium carrier gas. Various  $\text{Fe}_m\text{S}_n^-$  clusters were produced from the cluster source and were mass analyzed using a time-of-flight mass spectrometer. The  $\text{FeS}_n^-$  ( $n = 1-6$ ) species of our current interest were mass-selected and decelerated before being photodetached. Four detachment photon energies were used in the current experiments: 532 nm (2.331 eV), 355 nm (3.496 eV), and 266 nm (4.661 eV) from a Nd:YAG laser, and 193 nm (6.424 eV) from an ArF excimer laser. Photoelectrons were collected at nearly 100% efficiency by the magnetic bottle and analyzed in a 3.5 m long electron flight tube. The photoelectron spectra were calibrated using the known spectrum of  $\text{Rh}^-$ , and the resolution of the apparatus was  $\Delta E_k/E_k \sim 2.5\%$ , i.e.,  $\sim 25$  meV for 1 eV electrons. The electron binding energies (BE) were determined from the photoelectric equation:  $\text{BE} = h\nu - E_k$ .

## 3. Results

The obtained PES spectra for  $\text{FeS}_n^-$  ( $n = 1-6$ ) at different photon energies are shown in Figures 1–6, respectively. The observed detachment transitions are labeled with letters and the vertical lines represent the resolved vibrational structures. Figure 7 compares the spectra of all six species at 193 nm.

**3.1.  $\text{FeS}^-$ .** The PES spectra of  $\text{FeS}^-$  were measured at four photon energies, as shown in Figure 1. At the highest photon energy used (Figure 1d), six intense and well-resolved features (X, A–E) were observed, with several weak features (a–d).

The 532 nm spectrum (Figure 1a) revealed a long and well-resolved vibrational progression for the ground-state transition (X) with an average spacing of  $520 \pm 30 \text{ cm}^{-1}$ . The 0–0 transition was weak, defining an adiabatic detachment energy (ADE) of  $1.725 \pm 0.010 \text{ eV}$ , which represents the electron affinity (EA) of the neutral FeS molecule. The vertical detachment energy (VDE) was defined by the  $2 \leftarrow 0$  transition at  $1.851 \pm 0.010 \text{ eV}$ .

The 355 nm spectra (Figure 1b) revealed several more transitions. The feature A with a VDE of  $2.400 \pm 0.008 \text{ eV}$  was very sharp, only slightly broader than the instrumental resolution. The next low-lying transition (B) showed a simple and well-resolved vibrational progression with an average spacing of  $325 \pm 30 \text{ cm}^{-1}$ . The ADE for the B band was measured to be  $2.831 \pm 0.009 \text{ eV}$ . At the higher binding energy side of the 355 nm spectrum, numerous peaks were observed. The six peaks in band C appeared to consist of a vibrational progression, but their spacings are not equal. The first three peaks gave an average spacing of  $450 \pm 40 \text{ cm}^{-1}$ , whereas the three higher binding energy peaks yielded an average spacing of  $330 \pm 40 \text{ cm}^{-1}$ . The relative intensity of the C band increased at higher photon energies (Figure 1c,d), where a single unresolved band was observed due to the deterioration of spectral resolution at higher electron kinetic energies. A sharp peak at 3.32 eV (labeled b) was also observed in the 355 nm spectrum (Figure 1b), but its intensity seemed to be significantly reduced in the higher photon energy spectra.

At 266 nm, an intense and sharp peak (D) was observed at the high binding energy end with a VDE of  $4.413 \pm 0.010 \text{ eV}$ . In addition, numerous weak and diffuse features were observed between 3.4 and 4.4 eV. At 193 nm, one more sharp peak (E) was observed at a VDE of 4.66 eV. At higher binding energies beyond 4.7 eV, no intense transitions were revealed. There might be weak spectral features, but the signal-to-noise ratio was too poor to allow any definitive identification in the high binding energy range. The binding energies and vibrational frequencies for the major spectral features observed for  $\text{FeS}^-$  are summarized in Table 1, along with tentative assignments, which will be discussed later.

**3.2.  $\text{FeS}_2^-$ .** The PES spectra of  $\text{FeS}_2^-$  measured at three photon energies are shown in Figure 2. Six intense and well-resolved bands (X, A–E) were observed at 193 nm (Figure 2c). The relative intensities of the bands A, B, and C decreased at 266 nm (Figure 2b). These bands were rather congested and were not better resolved under the improved instrumental resolution afforded at 266 nm. However, the X band was resolved into several features under the improved resolution at 355 nm (Figure 2a). These peaks appeared to consist of a vibrational progression, but their spacings were not uniform, indicating that probably more than one vibrational mode was involved. The threshold peak in the 355 nm spectrum defined a relatively accurate EA for  $\text{FeS}_2$  at  $3.222 \pm 0.009 \text{ eV}$ , which is much higher than that of FeS. Close examination of the 355 nm spectrum revealed that very weak features ( $X'$  and  $A'$ ) were present in the lower binding energy side. These features, which accounted for about 1% of the intensity relative to that of the X band, depended on the source conditions slightly, but could not be completely eliminated. They were attributed to the existence of a minor isomer, with an ADE of  $2.05 \pm 0.09 \text{ eV}$  and a VDE of  $2.15 \pm 0.05 \text{ eV}$ , much lower than those of the main isomer. The binding energies of all the observed detachment transitions for  $\text{FeS}_2^-$  are given in Table 2.

**3.3.  $\text{FeS}_3^-$ .** The spectra of  $\text{FeS}_3^-$  are shown in Figure 3 at three photon energies. The 355 nm spectrum (Figure 3a)

**TABLE 1: Observed Adiabatic (ADE) and Vertical (VDE) Electron Binding Energies from the Photoelectron Spectra of FeS<sup>-</sup> and the Electronic Excitation Energies and Vibrational Frequencies Determined for FeS and Tentative Spectral Assignments<sup>a</sup>**

	state	electron configuration	ADE (eV)	VDE (eV)	term value (eV)	vib freq (cm <sup>-1</sup> )
X	<sup>5</sup> Δ	10σ <sup>2</sup> 4π <sup>4</sup> 11σ <sup>1</sup> 5π <sup>2</sup> 1δ <sup>3</sup> 12σ <sup>0</sup>	1.725 (10)	1.851 (10)	0	520 (30) <sup>b</sup>
A	<sup>7</sup> Σ <sup>+</sup>	10σ <sup>2</sup> 4π <sup>4</sup> 11σ <sup>1</sup> 5π <sup>2</sup> 1δ <sup>2</sup> 12σ <sup>1</sup>	2.400 (8)	2.400 (8)	0.675	
B	<sup>5</sup> Δ	10σ <sup>2</sup> 4π <sup>4</sup> 11σ <sup>0</sup> 5π <sup>2</sup> 1δ <sup>3</sup> 12σ <sup>1</sup>	2.831 (9)	2.867 (9)	1.106	325 (30)
C	<sup>5</sup> Π	10σ <sup>2</sup> 4π <sup>4</sup> 11σ <sup>1</sup> 5π <sup>1</sup> 1δ <sup>3</sup> 12σ <sup>1</sup>	3.025 (10)	3.079 (10)	1.300	450 (40)
	<sup>5</sup> Φ		3.150 (15)	3.195 (15)	1.425	330 (40)
D	<sup>7</sup> Φ	10σ <sup>2</sup> 4π <sup>3</sup> 11σ <sup>1</sup> 5π <sup>2</sup> 1δ <sup>3</sup> 12σ <sup>1</sup>	4.413 (10)	4.413 (10)	2.688	
E	<sup>7</sup> Δ	10σ <sup>1</sup> 4π <sup>4</sup> 11σ <sup>1</sup> 5π <sup>2</sup> 1δ <sup>3</sup> 12σ <sup>1</sup>	4.660 (20)	4.660 (20)	2.935	

<sup>a</sup> Numbers in the parentheses indicate the uncertainties of the last digits. <sup>b</sup> 540 cm<sup>-1</sup> from ref 8.

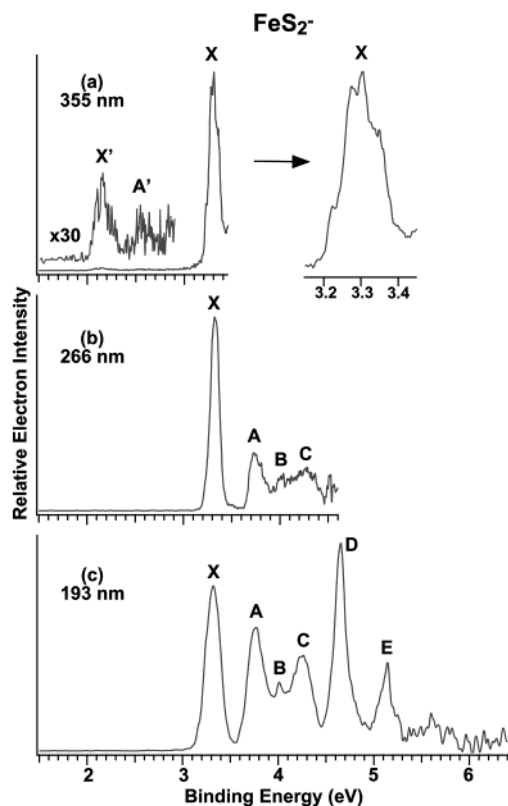


**Figure 2.** Photoelectron spectra of FeS<sub>2</sub><sup>-</sup> at (a) 355 nm, (b) 266 nm, and (c) 193 nm. The inset in (a) shows the fine structures of band X.

displayed surprisingly a simple and well-resolved vibrational progression for the ground-state transition (X) with a spacing of  $500 \pm 20$  cm<sup>-1</sup>. The 0–0 transition defined an accurate EA of  $2.898 \pm 0.008$  eV for neutral FeS<sub>3</sub>. At 266 nm, three strong bands (A, B, C) were observed with several weak features (a, b, c). The C band was relatively sharp, but fine features were discernible in the A and B bands, which can be due to either vibrational structures or overlapping electronic transitions. At 193 nm, a broad band (D) was observed between 4.9 and 5.5 eV, which likely contained several overlapping detachment transitions. The binding energies for the major detachment transition of FeS<sub>3</sub><sup>-</sup> are listed in Table 2.

**3.4. FeS<sub>4</sub><sup>-</sup>.** Figure 4 shows the PES spectra of FeS<sub>4</sub><sup>-</sup> at three photon energies. At 193 nm (Figure 4c), at least seven detachment bands could be identified (X, A–F). The A band appeared as a shoulder on the high binding energy side of band X, whereas the C, D, and E bands overlapped with each other. The F band at higher binding energies was relatively weak and contained at least four discernible features between 5.0 and 5.6 eV. The spacings between the fine features in the F band were too large to be due to a single vibrational progression. The X band was resolved into many fine features under the improved resolution at 355 nm (Figure 4a). At least seven fine features

**TABLE 2: Observed Electron Binding Energies (VDEs) for FeS<sub>n</sub><sup>-</sup> (n = 2–6), and Adiabatic Electron Affinities (EAs) and Vibrational Frequencies for FeS<sub>n</sub><sup>-</sup> (n = 2–6)<sup>a</sup>**

species	obsd feature	EA (eV)	VDE (eV)	vib freq (cm <sup>-1</sup> )	
FeS <sub>2</sub> <sup>-</sup>	X	3.222 (9)	3.306 (9)		
	A		3.75 (3)		
	B		4.01 (2)		
	C		4.25 (2)		
	D		4.66 (2)		
	E		5.15 (2)		
	X'	2.05 (9)	2.15 (5)		
FeS <sub>3</sub> <sup>-</sup>	X	2.898 (8)	2.898 (8)	500 (20)	
	A		3.348 (10)		
	B		4.156 (10)		
	C		4.40 (2)		
FeS <sub>4</sub> <sup>-</sup>	X	a	3.129 (8)	3.129 (8)	
		b		3.156 (9)	
		c		3.201 (8)	
		d		3.225 (8)	
		e		3.273 (8)	
		f		3.294 (8)	
		g		3.372 (8)	
	A		~3.5		
	B		3.94 (3)		
	C		~4.6		
FeS <sub>5</sub> <sup>-</sup>	X	3.262 (10)	3.262 (10)	510 (40)	
	A		3.55 (4)		
	B		4.72 (4)		
	C		5.32 (2)		
	D		~5.85		
	F		5.0–5.6		
FeS <sub>6</sub> <sup>-</sup>	X	3.52 (2)	3.52 (2)		
	A		~3.7		
	B		4.10 (3)		
	C		4.40 (3)		
D		4.62 (3)			

<sup>a</sup> The numbers in the parentheses represent the experimental uncertainty in the last digitals.

were identified (a–g). The threshold peak a was very sharp and defined an accurate EA of  $3.129 \pm 0.008$  eV for neutral FeS<sub>4</sub>. The fine features in the X band could be due to overlapping vibronic states. There appeared to be two vibrational progressions: one consisted of peak a, c, and e (average spacing,  $580 \pm 40$  cm<sup>-1</sup>) whereas the other one consisted of peak b, d, and f (average spacing,  $560 \pm 40$  cm<sup>-1</sup>). However, the peak f at 3.294 eV was significantly enhanced in the 266 nm spectrum (Figure 4b), suggesting that it may be a separate detachment channel. On the lower binding energy side in the 355 nm spectrum (Figure 4a), very weak signals were present, which were probably due to contributions from a minor isomer. The binding energies of all the observed features in the spectra of FeS<sub>4</sub><sup>-</sup> are also given in Table 2.

**3.5. FeS<sub>5</sub><sup>-</sup> and FeS<sub>6</sub><sup>-</sup>.** The PES spectra of FeS<sub>5</sub><sup>-</sup> were measured at three photon energies, as shown in Figure 5. The 193 nm spectrum (Figure 5c) exhibited five broad and intense

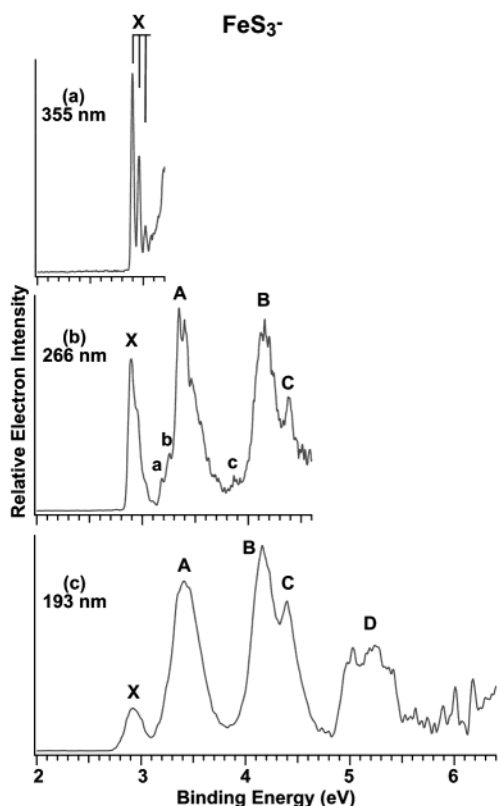


**Figure 3.** Photoelectron spectra of  $\text{FeS}_3^-$  at (a) 355 nm, (b) 266 nm, and (c) 193 nm. The vertical lines represent vibrational structures.

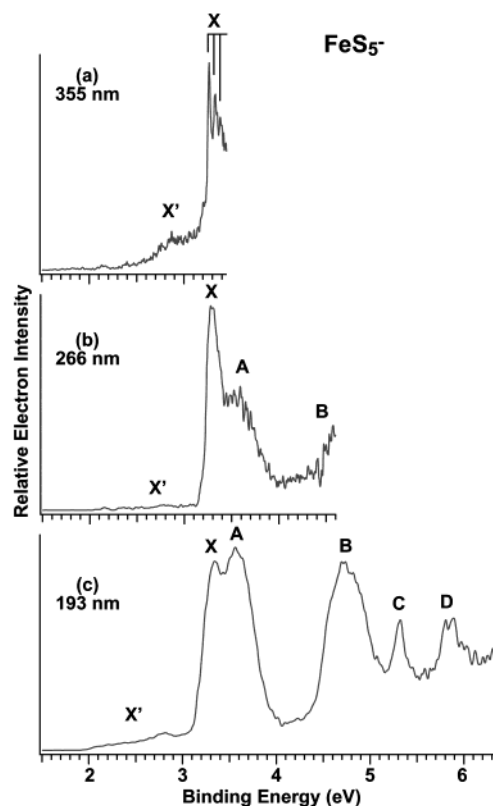


**Figure 5.** Photoelectron spectra of  $\text{FeS}_5^-$  at (a) 355 nm, (b) 266 nm, and (c) 193 nm.

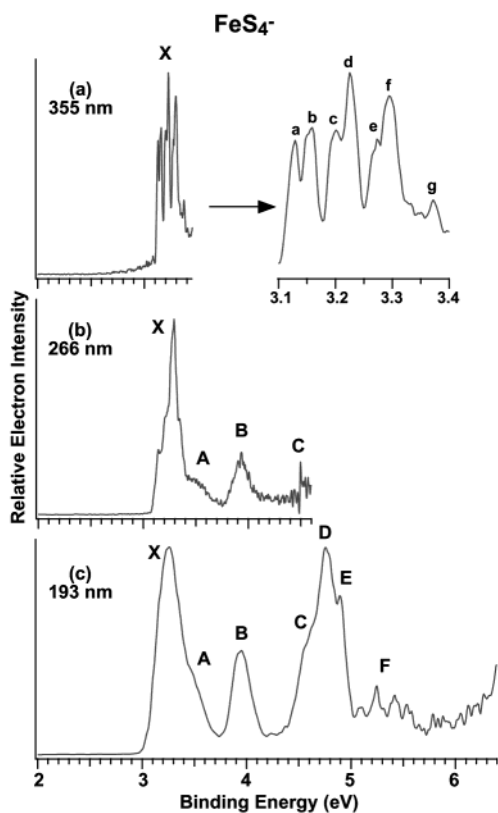


**Figure 4.** Photoelectron spectra of  $\text{FeS}_4^-$  at (a) 355 nm, (b) 266 nm, and (c) 193 nm. The inset in (a) shows the fine structures of band X.

bands (X, A–D). In the 355 nm spectrum (Figure 5a), a simple vibrational progression was resolved for the ground-state transition (X), with a spacing of  $510 \pm 40 \text{ cm}^{-1}$  and an ADE of  $3.262 \pm 0.010 \text{ eV}$ . The A band, which overlapped with the

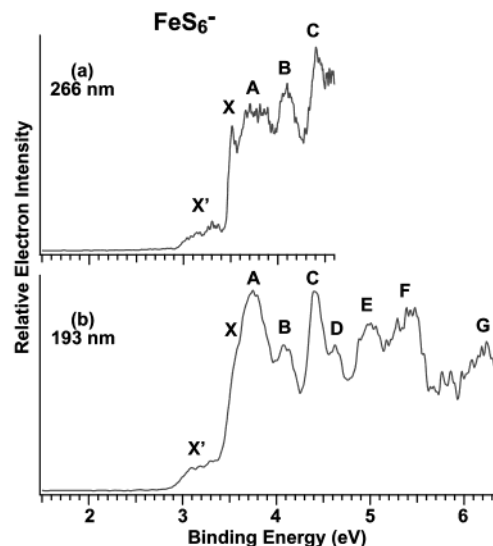


**Figure 6.** Photoelectron spectra of  $\text{FeS}_6^-$  at (a) 266 nm and (b) 193 nm.

X band, was enhanced in the 193 nm spectrum. The B, C, D bands have relatively high binding energies and were well separated from the A band. Weak features ( $X'$ ) at the lower binding energy side, due to the presence of a minor isomer, were observed in the spectra at all three photon energies. Again, the binding energies of the main detachment features of  $\text{FeS}_5^-$  are given in Table 2.

Due to its high electron binding energies, the spectra of  $\text{FeS}_6^-$  were taken only at 266 and 193 nm, as shown in Figure 6. Very congested and complex spectra were observed for  $\text{FeS}_6^-$ . The weak low binding energy features ( $X'$ ) between 3.0 and 3.4 eV were again attributed to contributions from a minor isomer. Thus, the X feature defines the ground-state transition of the

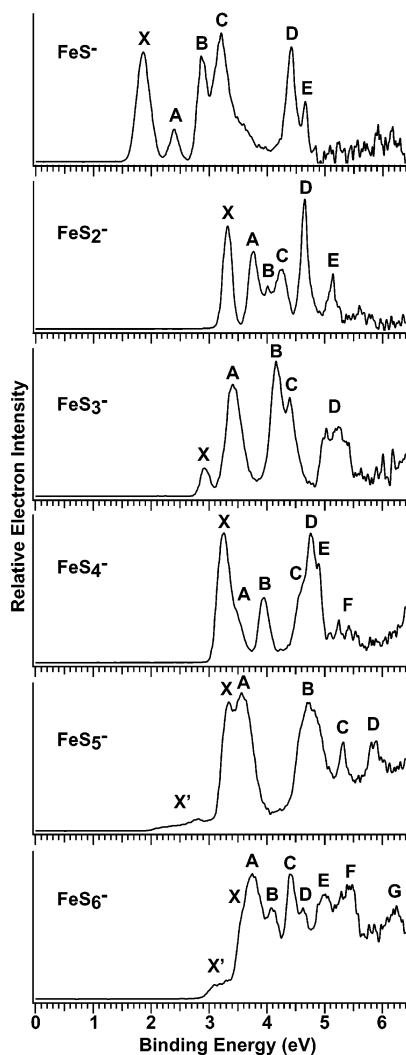


**Figure 7.** Comparison of the 193 nm photoelectron spectra of  $\text{FeS}_n^-$  ( $n = 1-6$ ).

main  $\text{FeS}_6^-$  isomer. This feature was well resolved in the 266 nm spectrum, yielding an ADE of  $3.52 \pm 0.02$  eV. All the higher energy features were broad, and Table 2 lists tentatively the binding energies for some of those bands.

#### 4. Discussion

The PES spectra shown in Figures 1–6 represent detachment transitions from the  $\text{FeS}_n^-$  anions to the various states of the  $\text{FeS}_n$  neutrals. They reveal information about the electronic structure and chemical bonding of the monoiron sulfur clusters. However, except for FeS and  $\text{FeS}_2$  there have been few theoretical studies on the structure and bonding of these species. In particular, the electronic structures of these species are extremely complex and very little is known for this series of species besides FeS. We will discuss the spectra of  $\text{FeS}^-$  in more detail and attempt to make some tentative assignments. For the larger clusters, we will discuss only qualitatively the trend of the spectra and the possible structural implications. No detailed spectral assignments are possible at present. We will also present a preliminary density functional theory (DFT) calculations for the species with  $n > 1$  to obtain structural information and provide insight into the bonding of the larger  $\text{FeS}_n$  clusters.

**4.1. Electronic Structure and Chemical Bonding in Diatomic  $\text{FeS}^-$  and FeS.** There have been a number of theoretical calculations on the electronic structure of FeS and  $\text{FeS}^-$ .<sup>21–25</sup>

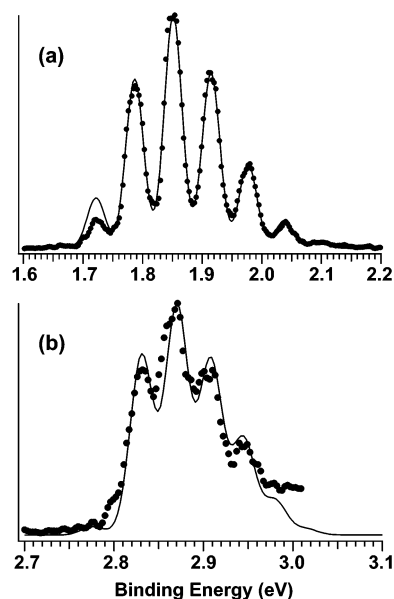


**Figure 8.** Franck–Condon factor simulations for (a) the X band and (b) the B bands of  $\text{FeS}^-$  (see Figure 1). The following parameters were used for the simulations: (a) anion frequency  $450\text{ cm}^{-1}$ , anharmonicity  $5\text{ cm}^{-1}$ , bond length  $2.18\text{ \AA}$ ; neutral frequency,  $540\text{ cm}^{-1}$ , anharmonicity,  $5\text{ cm}^{-1}$ , bond length,  $2.04\text{ \AA}$ ; anion vibrational temperature  $180\text{ K}$ ; line width  $35\text{ meV}$ ; (b) anion frequency  $450\text{ cm}^{-1}$ , anharmonicity  $5\text{ cm}^{-1}$ , bond length  $2.18\text{ \AA}$ ; neutral frequency  $325\text{ cm}^{-1}$ , anharmonicity  $5\text{ cm}^{-1}$ , bond length  $2.29\text{ \AA}$ ; anion vibrational temperature  $180\text{ K}$ ; line width  $30\text{ meV}$ .

The ground state of FeS is known to be  $^5\Delta$  with an electron configuration of  $10\sigma^2 4\pi^4 11\sigma^1 5\pi^2 1\delta^3$ , where the  $10\sigma$  and  $4\pi$  are weakly bonding MOs mainly of S  $3p$  character, the  $11\sigma$  is a bonding MO mainly of Fe  $3d$  character, the  $5\pi$  is an antibonding MO of Fe  $3d$  character, and the  $1\delta$  is an Fe  $3d$  nonbonding MO. The recent calculations by Hubner et al. give a  $^5\Sigma^+$  ground state for  $\text{FeS}$ ,<sup>25</sup> but the  $^5\Delta$  state is predicted to be very closely spaced and the energy difference between the two states is well within the accuracy of the calculations. In the  $\text{FeS}^-$  anion, the extra electron enters the  $12\sigma$  orbital, which is an antibonding MO mainly of Fe  $4s$  character, to give a  $^6\Delta$  state with an electron configuration of  $10\sigma^2 4\pi^4 11\sigma^1 5\pi^2 1\delta^3 12\sigma^1$ . Because there is little experimental information about the excited states of FeS, we will use the available theoretical information as guidance to give tentative assignments of the major observed PES features.

**4.1.1. Ground-State Transition (X) and Franck–Condon Factor Simulations.** Feature X represents detachment of the extra electron from the  $12\sigma$  MO of the anion, leading to the neutral ground state ( $^5\Delta$ ). The broad vibrational progression is consistent with the antibonding nature of the  $12\sigma$  orbital. Our observed average vibrational spacing of  $520 \pm 30\text{ cm}^{-1}$  is in excellent agreement with the known vibrational frequency of FeS ( $540\text{ cm}^{-1}$ ).<sup>8</sup> The well-resolved vibrational progression for the ground state afforded us an opportunity to perform a Franck–Condon factor simulation,<sup>27</sup> which would confirm the spectroscopic constants of the ground states of  $\text{FeS}^-$  and FeS and allow us to estimate the vibrational temperature of  $\text{FeS}^-$ . We should point out that the  $^5\Delta$  state should have a significant spin–orbit splitting yielding a doublet for each vibrational peak in the PES spectra of the X band. However, the spin–orbit components were not resolved due to the limited resolution. The line width of the 532 nm spectrum (Figure 1a) was about  $35\text{ meV}$  (fwhm), which was broader than our instrumental resolution, most likely as a result of the spin–orbit broadening.

Figure 8a displays the simulated spectrum, using a Morse oscillator,<sup>27</sup> compared to the experimental data. We used the

known vibrational frequency ( $540\text{ cm}^{-1}$ )<sup>8</sup> and bond length ( $2.04\text{ \AA}$ )<sup>25</sup> of the neutral ground state and a  $5\text{ cm}^{-1}$  anharmonicity for both the anion and the neutral. The simulation yielded a bond length of  $2.18\text{ \AA}$  and a vibrational frequency of  $450\text{ cm}^{-1}$  for the  $\text{FeS}^-$  anion, which are in good agreement with those calculated recently.<sup>25</sup> The anion vibrational frequency for  $\text{FeS}^-$  is only an estimate because there is very little hot band transition. Most interestingly, we obtained a vibrational temperature of  $180\text{ K}$  for  $\text{FeS}^-$ , the coldest vibrational temperature that we have been able to achieve from our laser vaporization source.<sup>28,29</sup>

**4.1.2. The A, B, and C Bands.** The A band is very sharp without any vibrational structures and is clearly from removal of a nonbonding electron. It should be due to detachment of a  $1\delta$  electron unambiguously, yielding the  ${}^7\Sigma^+$  excited state of  $\text{FeS}$  at an excitation energy of  $0.675\text{ eV}$  relative to the ground state (Table 1). The sharp detachment peak of the A band suggests that the bond length and vibrational frequency of the  ${}^7\Sigma^+$  excited state should be very similar or nearly identical to those of the anion ground state.

The band B exhibited a single vibrational progression with a frequency of  $325\text{ cm}^{-1}$ , which is much smaller than that of the ground state of either the neutral or the anion, indicating the detachment of a strongly bonding electron. We assign this band to the detachment of the  $11\sigma$  orbital, an Fe–S bonding MO, yielding the  ${}^5\Delta$  excited state of  $\text{FeS}$  with an excitation energy of  $1.106\text{ eV}$  (Table 1). Using the spectroscopic constants and the vibrational temperature of the anion ground state, we performed a Franck–Condon factor simulation similar to that for the X band, as shown in Figure 8b. We obtained a bond length of  $2.29\text{ \AA}$  for the  ${}^5\Delta$  excited state of  $\text{FeS}$  from the Franck–Condon factor simulation. Figure 8b shows that there appeared to be a lower binding energy component in each vibrational peak, possibly due to the spin–orbit splitting expected for the  ${}^5\Delta$  excited state.

The C band is more complicated and not straightforward to assign. In the  $266\text{ nm}$  spectrum, numerous vibronic peaks were resolved in this band, which appeared to contain two vibrational progressions. This band is tentatively assigned to be due to detachment from the  $5\pi$  orbital, yielding the  ${}^5\Pi$  and  ${}^5\Phi$  excited states of  $\text{FeS}$ , both of which can be produced from a single electron detachment from the  $5\pi$  orbital.

**4.1.3. D and E Bands.** The next strong detachment feature is the D band at an ADE of  $4.413\text{ eV}$ . We assign this feature to be from detachment of a  $4\pi\beta$  electron, giving rise to the  ${}^7\Phi$  excited state of  $\text{FeS}$  at an excitation energy of  $2.688\text{ eV}$  (Table 1). This band is quite sharp without significant vibrational structures, suggesting that the  $4\pi$  orbital is relatively nonbonding. The band E with the highest binding energy could be either due to the  ${}^5\Phi$  state from detachment of a  $4\pi\alpha$  electron or due to detachment of a  $10\sigma\beta$  electron, yielding a  ${}^7\Delta$  excited state of  $\text{FeS}$ . We tentatively assigned the E band to the latter, as shown in Table 1.

**4.1.4. Weak PES Features.** The above assignments accounted for all the major PES features observed for  $\text{FeS}^-$ . It is expected that there would be many low-lying excited states for  $\text{FeS}$  with different spins or angular momenta. However, only those states that involve detachment of a single electron from the anion ground state would give strong PES features. States involving excitations of more than one electron would have much weaker intensities. The relatively weak features (a–d) observed in the spectra of  $\text{FeS}^-$  are attributed to such multielectron transitions.

Our overall spectral assignments are given in Table 1. All but the X, A, and B bands should be regarded as tentative. We note that our assignments differ significantly from those by Hubner et al.<sup>25</sup> However, those assignments were based on a poorly resolved spectrum<sup>20</sup> and were problematic in themselves.

For example, three distinct electronic states ( ${}^5\Sigma^+$ ,  ${}^5\Delta$ ,  ${}^7\Sigma^+$ ) were assigned to the X band on the basis of shoulders observed in the previous spectrum. Our data showed clearly that the X band contains only one vibrational progression. On the basis of the nature of the MOs and the geometry and vibrational frequency changes, we consider the assignments of the X, A, and B states reasonably firm. Our spectra and the Franck–Condon factor simulations yielded a set of spectroscopic constants for these three states, which should provide good experimental references to verify further and more accurate theoretical calculations.

**4.2.  $\text{FeS}_2^-$  and  $\text{FeS}_2$ .** Two structures are possible for  $\text{FeS}_2$ , a bent structure without S–S bonding or a triangular structure with a S–S bond. The recent work by Schröder et al. reported an extensive experimental and theoretical investigation on the structures of  $\text{FeS}_2^{+/0/-}$ .<sup>13</sup> Their DFT calculation showed that  $\text{FeS}_2^-$  has a bent structure ( ${}^6A_1$ ) with a  $\angle\text{SFeS}$  angle of  $166.7^\circ$  and an Fe–S bond length of  $2.12\text{ \AA}$ . Their predicted neutral  $\text{FeS}_2$  also has a bent structure ( ${}^5B_2$ ), but it has a large bond angle change ( $\angle\text{SFeS} = 115.2^\circ$ ), as well as a bond length change ( $r_{\text{Fe-S}} = 2.03\text{ \AA}$ ).

The X band in the PES spectrum of  $\text{FeS}_2^-$  (Figure 2) represents the transition from the ground state of the anion to that of the neutral. Our spectrum at  $355\text{ nm}$  (Figure 2a) revealed partially resolved vibrational structures. The fact that no single vibrational progression was observed suggested that there is more than one active vibrational mode. Most likely, the bending and symmetric stretching modes were both active. This observation is consistent with the calculated structural changes between the anion and neutral ground state of  $\text{FeS}_2$  by Schröder et al.<sup>13</sup> Interestingly, their calculated relative energies between the anion and neutral is  $3.30\text{ eV}$ , which is in excellent agreement with our measured EA of  $3.222\text{ eV}$  for  $\text{FeS}_2$  (Table 2). However, the sharp spectral features observed in the X band did not suggest a large bond angle change as predicted by Schröder et al.

The EA of  $\text{FeS}_2$  is quite high, suggesting that the  $\text{FeS}_2^-$  anion is very stable. This is understandable, because in  $\text{FeS}_2^-$  the Fe and S are both in their favorite oxidation state; i.e.,  $\text{FeS}_2^-$  can be viewed as  $\text{S}^{2-}\text{Fe}^{3+}\text{S}^{2-}$  in a formal sense. The five d electrons in  $\text{Fe}^{3+}$  are high spin coupled, giving rise to the  ${}^6A_1$  ground state. The quintet ground state of  $\text{FeS}_2$  ( ${}^5B_2$ ) implies that the removed electron is mainly of Fe 3d character. The change of the Fe–S bond length suggests that there is significant covalent interaction between the Fe 3d orbitals and the S 3p. We note that the PES spectra of  $\text{FeS}_2^-$  are similar to those of its valent isoelectronic  $\text{FeO}_2^-$  species,<sup>30,31</sup> which also has a similar bent structure. However, it is surprising that the EA of  $\text{FeS}_2$  is even higher than that of  $\text{FeO}_2$  ( $2.36\text{ eV}$ ),<sup>30,31</sup> consistent with the fact that the Fe–S interaction is more covalent than the Fe–O bond.

The very weak feature (X') observed at the lower binding energy side of the  $\text{FeS}_2^-$  spectrum (Figure 2a) is assigned to the triangular isomer of  $\text{FeS}_2^-$  with a S–S bond. The lower EA of this isomer is expected and is consistent with the theoretical calculation by Schröder et al.,<sup>13</sup> who predicted a vertical EA of  $1.71\text{ eV}$  for the triangular isomer.

**4.3.  $\text{FeS}_3^-$  to  $\text{FeS}_6^-$ : Electron Binding Energy Trend and Implication for Structural Evolution.** The  $355\text{ nm}$  PES spectrum of  $\text{FeS}_3^-$  (Figure 3a) exhibited a simple vibrational progression with a frequency of  $500\text{ cm}^{-1}$ . This frequency is comparable to that of the diatomic  $\text{FeS}$  and should be due to an Fe–S symmetric stretching mode. The simple vibrational progression suggests that the ground states of  $\text{FeS}_3^-$  and  $\text{FeS}_3$  may possess rather high symmetry. There are two possible structures, either a  $D_{3h}$  structure without any S–S bonding or a  $C_{2v}$  structure with one S–S bond, a  $\text{SFe}(\text{S}_2)$  type of structure. In the  $D_{3h}$  structure, the  $500\text{ cm}^{-1}$  mode would correspond to the totally symmetric stretching, whereas in the  $C_{2v}$  structure

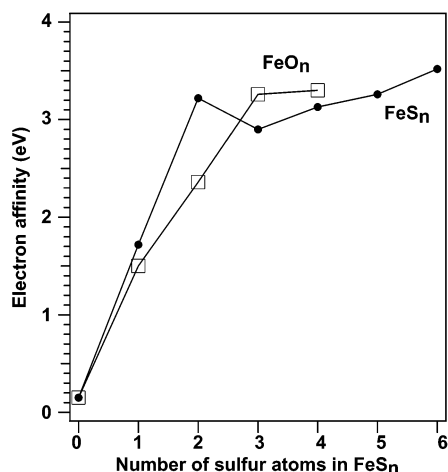


**Figure 9.** Electron affinities of  $\text{FeS}_n$  (filled dots) as a function of  $n$  compared to those of  $\text{FeO}_n$  from ref 31 (empty squares). The EA for Fe atom is taken from ref 40.

this mode could correspond to the stretching of the  $\text{SFe}$  moiety in  $\text{SFe}(\text{S}_2)$ . We expected that the  $D_{3h}$  structure would have a higher electron affinity, whereas the  $C_{2v}$  structure would have an EA comparable to that of  $\text{FeS}_2$ .

Interestingly, we observed that the EA of  $\text{FeS}_3$  is even smaller than that of  $\text{FeS}_2$  (Table 2). This is very different from the EA trend from  $\text{FeO}_2$  to  $\text{FeO}_3$ , which exhibits a large increase from the EA of 2.36 eV for  $\text{FeO}_2$  to 3.26 eV for  $\text{FeO}_3$ .<sup>31</sup> This was interpreted as a sequential oxidation, in that the Fe is further oxidized in  $\text{FeO}_3$  relative to  $\text{FeO}_2$ , and a  $D_{3h}$  structure was proposed for  $\text{FeO}_3$ .<sup>31</sup> The current observation of a decrease in EA from  $\text{FeS}_2$  to  $\text{FeS}_3$  suggests that the Fe is not further oxidized in the latter, favoring the  $C_{2v}$  structure for  $\text{FeS}_3$ . This is understandable because oxygen is expected to be a stronger oxidizer and the Fe–O bond is expected to be more ionic than the Fe–S bond. Therefore, Fe prefers its favorite +3 oxidation state in  $\text{FeS}_3^-$ , which can be viewed formally as  $\text{S}^{2-}\text{Fe}^{3+}(\text{S}_2^{2-})$ .

Figure 7 shows all the PES data of  $\text{FeS}_n^-$  ( $n = 1-6$ ) at 193 nm. We note that the electron binding energies of the larger clusters ( $n > 3$ ) are in general similar to those of  $\text{FeS}_2^-$  and  $\text{FeS}_3^-$ . Figure 9 plots the trend of the EA as a function of  $n$  for  $\text{FeS}_n$ , compared with that of  $\text{FeO}_n$ .<sup>31</sup> It is clear that the EAs of  $\text{FeS}_{4-6}$  are similar to that of  $\text{FeS}_2$  without any significant increase, suggesting that Fe is likely to maintain its favorite

+3 oxidation state in all these clusters with  $(\text{S}_m^{2-})\text{Fe}^{3+}(\text{S}_{n-m}^{2-})$  types of structures. For example,  $\text{FeS}_4^-$  may be either  $\text{S}_2^{2-}\text{Fe}^{3+}\text{S}_2^{2-}$  or  $\text{S}^{2-}\text{Fe}^{3+}\text{S}_3^{2-}$ . The trend of the EA for the  $\text{FeO}_n$  series is consistent with the above structural evolution. The EA of  $\text{FeO}_4$  is similar to that of  $\text{FeO}_3$ , suggesting the onset of an O–O unit in  $\text{FeO}_4^-$ , which was experimentally confirmed.<sup>31</sup> In the following section, we present a preliminary DFT calculations, which generally confirm the above structural evolution for the larger  $\text{FeS}_n^-$  clusters.

**4.4. Preliminary DFT Calculations.** Accurate prediction of various electronic states of Fe–S systems is a considerable challenge to computational chemistry, due to the existence of near degenerate states and low-lying geometrical isomers. We are interested in a detailed understanding of the electronic structure and chemical bonding of Fe–S clusters using DFT. Although detailed calculations will be presented in a forthcoming paper,<sup>32</sup> here we wish to report structural results from our DFT calculations. DFT has been very successful in electronic structure calculations of transition metals and had become a default choice.<sup>33</sup> Despite this phenomenal success, DFT is still a single determinant method and cannot account for static correlation effects, arising from near degenerate electronic states, which are important for Fe–S systems. Therefore, our aim in the current preliminary study is to identify various low-lying isomers of  $\text{FeS}_n^-$ , which can be used later for more accurate calculations.

All calculations were done with ADF<sup>34,35</sup> at the level of generalized gradient approach using Perdew–Wang exchange–correlation functional<sup>36,37</sup> at the unrestricted level. Slater-type-orbital (STO) basis sets of triple- $\zeta$  plus polarization (TZP) functions were used for both Fe and S atoms without any frozen core approximation (i.e., all electron calculations). The geometries of all the molecules were fully optimized with the default parameters.

Structures of the two low-lying isomers for each  $\text{FeS}_n^-$  species are presented in Figure 10, along with their relative energies and bond lengths. We first examine the DFT results for  $\text{FeS}^-$ . In contrast to the  $^4\Delta$  ground state of  $\text{FeO}^-$ ,<sup>30,38,39</sup> calculations by Hubner et al. gave a  $^6\Delta$  ground state for  $\text{FeS}^-$  with a 2.16 Å bond length.<sup>25</sup> Our DFT calculations also predict the  $^6\Delta$  ground state for  $\text{FeS}^-$  with a bond length of 2.13 Å and a configuration of  $10\sigma^2 4\pi^4 11\sigma^1 5\pi^2 1\delta^3 12\sigma^1$ . However, both our calculations and the previous DFT calculations with large basis set predict a  $^5\Delta$  ground state for  $\text{FeS}^-$ .<sup>25</sup> According to our study,

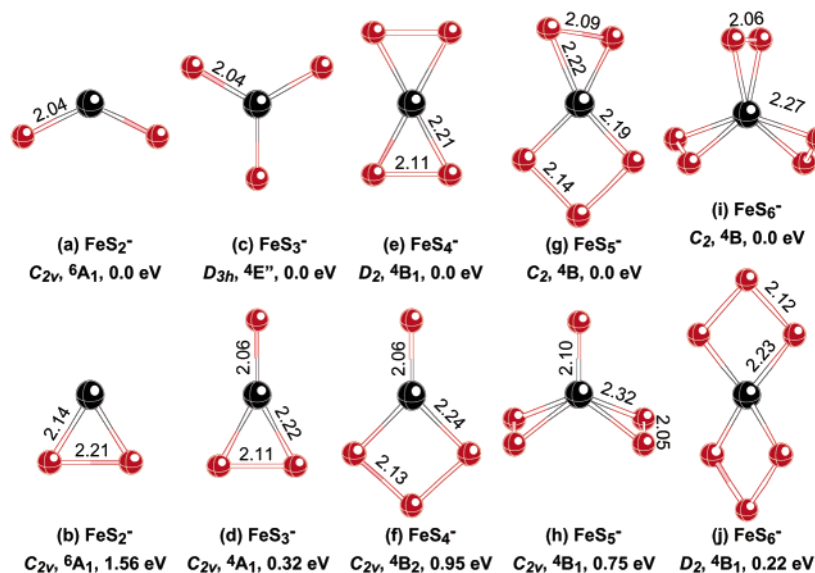


**Figure 10.** Structures and low-lying isomers of  $\text{FeS}_n^-$  ( $n = 2-6$ ) from density functional calculations.

the highest singly occupied molecular orbitals of  $\text{FeS}^-$  are the  $1\delta\beta$  and  $12\sigma^1\alpha$  MOs, which are closely spaced. Detachment from the  $12\sigma$  and  $1\delta$  MOs results in the  $^5\Delta$  ground state and the  $^7\Sigma^+$  excited state of  $\text{FeS}$ , respectively, consistent with our spectral assignments.

However, ground state predictions become more complicated for other members of the series. Not only various electronic states but also different geometrical isomers become competitive. For  $\text{FeS}_2^-$ , we obtained a bent ground state (Figure 10a), which is in agreement with the previous DFT calculations by Schröder et al.<sup>13</sup> The triangular isomer (Figure 10b) is about 1.56 eV higher in energy. For  $\text{FeS}_3^-$ , our DFT calculations gave two isomers (Figure 10c,d) very close in energy, with the  $D_{3h}$  structure (Figure 10c) slightly more stable than the  $C_{2v}$  isomer (Figure 10d). It is not clear which one is the ground state, because it is well-known that DFT overestimates the stabilization of delocalized structures, but the  $C_{2v}$  isomer is consistent with our experimental results. For both  $\text{FeS}_4^-$  and  $\text{FeS}_5^-$ , our calculations give the  $D_2$  (Figure 10e) and  $C_2$  (Figure 10g) ground states, which are more stable than the closest isomers by 0.95 and 0.75 eV, respectively. However, the two isomers for  $\text{FeS}_6^-$  (Figure 10i,j) are very close in energy, making it difficult to ascertain which one is the ground state.

One important feature that distinguishes between oxides and sulfides is that the sulfides are more covalent. Our preliminary charge analyses of the  $\text{FeS}_n^-$  series indicate that there is little charge polarization among the Fe and S atoms. Overall, the DFT results are consistent with the  $(S_m^{2-})\text{Fe}^{3+}(S_{n-m}^{2-})$  types of structures proposed on the basis of the experimental results. A detailed theoretical study on the  $\text{FeS}_n^-$  clusters is forthcoming.<sup>32</sup>

## 5. Conclusions

In conclusion, we report a photoelectron spectroscopic investigation of a series of monoiron-sulfur clusters  $\text{FeS}_n^-$  ( $n = 1-6$ ) at four photon energies. Vibrationally resolved spectra were obtained for  $\text{FeS}^-$  and  $\text{FeS}_3^-$ , and well-resolved spectra with numerous features were obtained for all  $\text{FeS}_n^-$  species. Detailed electronic energy level information is obtained for  $\text{FeS}$  from the PES data of  $\text{FeS}^-$  and tentative assignments are presented. Sequential oxidation of Fe was observed only for the first two S atoms, where each S atom is responsible for a large increase of electron affinity of  $\sim 1.6$  and  $\sim 1.5$  eV, respectively. All larger species  $\text{FeS}_n$  ( $n = 3-6$ ) were observed to possess electron affinities similar to that of  $\text{FeS}_2$  within  $\pm 0.3$  eV. On the basis of the EA trend, a general structural evolution scheme is proposed, where all  $\text{FeS}_n^-$  ( $n > 1$ ) species take the  $(S_m^{2-})\text{Fe}^{3+}(S_{n-m}^{2-})$  type structures, in which Fe maintains its favorite +3 oxidation state. Preliminary DFT calculations were carried out, which, in general, verify the proposed structural types for  $\text{FeS}_n^-$ .

**Acknowledgment.** We thank Dr. Jun Li for invaluable discussions and assistance in the theoretical calculations. This research was supported by the National Institutes of Health (GM-63555) and partially by the Petroleum Research Fund, administered by the American Chemical Society. The experiment was performed at the W. R. Wiley Environmental Molecular Sciences Laboratory, a national scientific user facility sponsored by DOE's Office of Biological and Environmental Research and located at Pacific Northwest National Laboratory, operated for DOE by Battelle. All the calculations were performed using supercomputers at EMSL MSCF.

## References and Notes

- Beinert, H.; Holm, R. H.; Munck, E. *Science* **1997**, *277*, 653.
- Ogino, H.; Inomata, S.; Tobita, H. *Chem. Rev.* **1998**, *98*, 2093.
- Harris, S. *Polyhedron* **1989**, *8*, 2843.
- Noodleman, L.; Peng, C. Y.; Case, D. A.; Mousesca, J.-M. *Coord. Chem. Rev.* **1995**, *144*, 199.
- Mousesca, J.-M.; Lamotte, B. *Coord. Chem. Rev.* **1998**, *178-180*, 1573.
- Wang, L. S.; Cheng, H. S.; Fan, J. J. *J. Chem. Phys.* **1995**, *102*, 9480. Wang, L. S.; Wu, H. In *Advances in Metal and Semiconductor Clusters. IV. Cluster Materials*; Duncan, M. A., Ed.; JAI Press: Greenwich, 1998; pp 299-343.
- Wang, L. S.; Ding, C. F.; Wang, X. B.; Barlow, S. E. *Rev. Sci. Instrum.* **1999**, *70*, 1957.
- DeVore, T. C.; Franzen, H. F. *High Temp. Sci.* **1975**, *7*, 220.
- Barsch, S.; Kretzschmar, I.; Schröder, D.; Schwarz, H.; Armentrout, P. B. *J. Phys. Chem. A* **1999**, *103*, 5925.
- Barsch, S.; Schroder, D.; Schwarz, H.; Armentrout, P. B. *J. Phys. Chem. A* **2001**, *105*, 2005.
- Hettich, R. L.; Jackson, T. C.; Stanko, E. M.; Freiser, B. S. *J. Am. Chem. Soc.* **1986**, *108*, 5086.
- Husband, J.; Aguirre, F.; Thompson, C. J.; Metz, R. B. *Chem. Phys. Lett.* **2001**, *342*, 75.
- Schröder, D.; Kretzschmar, I.; Schwarz, H.; Rue, C.; Armentrout, P. B. *Inorg. Chem.* **1999**, *38*, 3474.
- Carlin, T. J.; Wise, M. B.; Freiser, B. S. *Inorg. Chem.* **1981**, *20*, 2743.
- Dance, I.; Fisher, K.; Willett, G. *Angew. Chem., Int. Ed. Engl.* **1995**, *34*, 201.
- Dance, I.; Fisher, K.; Willett, G. *Inorg. Chem.* **1996**, *35*, 4177.
- MacMahon, T. J.; Jackson, T. C.; Freiser, B. S. *J. Am. Chem. Soc.* **1989**, *111*, 421.
- Yu, Z.; Zhang, N.; Wu, X.; Gao, Z.; Zhu, Q.; Kong, F. *J. Chem. Phys.* **1993**, *99*, 1765.
- Nakat, J. E.; Fisher, K. J.; Dance, I. G.; Willett, G. D. *Inorg. Chem.* **1993**, *32*, 1931.
- Zhang, N.; Hayase, T.; Kawamata, H.; Nakao, K.; Nakajima, A.; Kaya, K. *J. Chem. Phys.* **1996**, *104*, 3413. Nakajima, A.; Hayase, T.; Hayakawa, F.; Kaya, K. *Chem. Phys. Lett.* **1997**, *280*, 381.
- Anderson, A. B.; Hong, S. Y.; Smialek, J. L. *J. Phys. Chem.* **1987**, *91*, 4250.
- Bauschlicher, Jr., C. W.; Maitre, P. *Theor. Chim. Acta.* **1995**, *90*, 189.
- Bridgeman, A. J.; Rothery, J. *J. Chem. Soc., Dalton Trans.* **2000**, *2*, 211.
- Glukhovtsev, M. N.; Bach, R. D.; Nagel, C. J. *J. Phys. Chem. A* **1997**, *101*, 316.
- Hubner, O.; Termath, V.; Berning, A.; Sauer, J. *Chem. Phys. Lett.* **1998**, *294*, 37.
- Hubner, O.; Sauer, J. *J. Chem. Phys.* **2002**, *116*, 617.
- Wang, L. S.; Niu, B.; Lee, Y. T.; Shirley, D. A.; Balasubramanian, K. *J. Chem. Phys.* **1990**, *92*, 899.
- Akola, J.; Manninen, M.; Hakkinen, H.; Landman, U.; Li, X.; Wang, L. S. *Phys. Rev. B* **1999**, *60*, 11297.
- Wang, L. S.; Li, X. Temperature Effects in Anion Photoelectron Spectroscopy of Metal Clusters. In *Clusters and Nanostructure Interfaces*; Jena, P.; Khanna, S. N.; Rao, B. K., Eds.; World Scientific: New Jersey, 2000; p 293.
- Fan, J.; Wang, L. S. *J. Chem. Phys.* **1995**, *102*, 8714.
- Wu, H.; Desai, S. R.; Wang, L. S. *J. Am. Chem. Soc.* **1996**, *118*, 5296, 7434.
- Kiran, B.; Li, J.; Zhai, H. J.; Wang, L. S. Manuscript to be published.
- Ziegler, T. *Chem. Rev.* **1991**, *91*, 651.
- ADF 2002, SCM, Theoretical Chemistry, Vrije Universiteit, Amsterdam, The Netherlands (<http://www.scm.com>). te Velde, G.; Bickelhaupt, F. M.; van Gisbergen, S. J. A.; Guerra, C. F.; Baerends, E. J.; Snijders, J. G.; Ziegler, T. *J. Comput. Chem.* **2001**, *22*, 931.
- Guerra, C. F.; Snijders, J. G.; te Velde, G.; Baerends, E. J. *Theor. Chem. Acc.* **1998**, *99*, 391.
- Perdew, J. P.; Wang, Y. *Phys. Rev. B* **1992**, *45*, 13244.
- Perdew, J. P.; Chevary, J. A.; Vosko, S. H.; Jackson, K. A.; Pederson, M. R.; Singh, D. J.; Foilhais, C. *Phys. Rev. B* **1992**, *46*, 6671.
- Dolg, M.; Wedig, U.; Stoll, H.; Preuss, H. *J. Chem. Phys.* **1987**, *86*, 2123.
- Krauss, M.; Stevens, W. J. *J. Chem. Phys.* **1985**, *82*, 5584.
- Leopold, D. G.; Lineberger, W. C. *J. Chem. Phys.* **1986**, *85*, 51.